CrossMark

HEAD AND NECK

Preliminary study of diffusion kurtosis imaging in thyroid nodules and its histopathologic correlation

Ruo-yang Shi[1] · Qiu-ying Yao[1] · Qin-yi Zhou[2] · Qing Lu[1] · Shi-teng Suo[1] · Jun Chen[2] ·
Wen-jie Zheng[2] · Yong-ming Dai[3] · Lian-ming Wu[1] · Jian-rong Xu[1]

Abstract

Objectives To evaluate the utility of diffusion kurtosis imaging (DKI) of patients with thyroid nodules and to assess the probable correlation with histopathological factors.

Methods The study included 58 consecutive patients with thyroid nodules who underwent magnetic resonance imaging (MRI) examination, including DKI and diffusion-weighted imaging (DWI). Histopathological analysis of paraffin sections included cell density and immunohistochemical analysis of Ki-67 and vascular endothelial growth factor (VEGF). Statistical analyses were performed using Student's t-test, receiver operating characteristic (ROC) curves and Spearman's correlation.

Results The diffusion parameters, cell density and immunohistochemistry analysis between malignant and benign lesions showed significant differences. The largest area under the ROC curve was acquired for the D value (AUC = 0.797). The highest sensitivity was shown with the use of K (threshold = 0.832, sensitivity = 0.917). The Ki-67 expression generally stayed low. A moderate correlation was found between ADC, D and cell density (r = −0.536, P = 0.000; r = −0.570, P = 0.000) and ADC, D and VEGF expression (r = −0.451, P = 0.000; r = −0.522, P = 0.000).

Conclusion The DKI-derived parameters D and K demonstrated an advantage compared to conventional DWI for thyroid lesion diagnosis. While the histopathological study indicated that the D value correlated better with extracellular change than the ADC value, the K value probably changed relative to the intracellular structure.

Key Points
• *DWI and DKI parameters can identify PTC from benign thyroid nodules.*
• *Correlations were found between diffusion parameters and histopathological analysis.*
• *DKI obtains better diagnostic accuracy than conventional DWI.*

Keywords Thyroid nodule · Thyroid · DWI · DKI · VEGF

Ruo-yang Shi and Qiu-ying Yao contributed equally to this work.

✉ Lian-ming Wu
  wlmssmu@126.com

✉ Jian-rong Xu
  xujrrj@163.com

1 Department of Radiology, Ren Ji Hospital, School of Medicine, Shanghai Jiao Tong University, No. 160, Pujian Road, Shanghai 200127, China

2 Department of Head and Neck Surgery, Ren Ji Hospital, School of Medicine, Shanghai Jiao Tong University, Shanghai, China

3 Magnetic Resonance Imaging Institute for Biomedical Research, Wayne State University, Detroit, MI, USA

Introduction

Reported thyroid malignancies have significantly increased in the last few decades [1]. Most thyroid malignancies include papillary (PTC), follicular (FTC), medullary (MTC) and anaplastic (ATC) thyroid carcinomas. Imaging modalities, including ultrasonography (US), computed tomography (CT) and magnetic resonance imaging (MRI), have been widely used for patients with thyroid lesions. Ultrasound is the most common imaging modality due to its convenience, but diagnosis varies according to the examining physician. Several guidelines have been published utilizing ultrasound criteria for the management of thyroid nodules that on morphological features [2]. However, as an imaging modality, MRI provides high soft tissue resolution, and various quantitative parameters

Table 1 Imaging protocol of conventional diffusion-weighted imaging (DWI) and diffusion kurtosis imaging (DKI)

Parameter	DWI	DKI
Pulse sequence	Single-shot echo planar	Single-shot echo planar
TR (ms)	3046	3046
TE (ms)	83	83
Field of view (mm^2)	270×206	270×206
Acquisition matrix	136×133	136×133
Bandwidth (Hz/voxel)	1,812	1,812
Slice thickness (mm)	4	4
b values (s/mm^2)	0, 750	0, 500, 1,000, 1,500, 2,000
Averages	4	4 (0, 500), 6 (1,000–2,000)

have already been used in thyroid lesion studies. However, most of the thyroid MRI studies concentrated on diffusion-weighted imaging (DWI) [3–9].

DWI has been widely used in clinical oncological diagnosis to indicate the conspicuity of the neoplasm against a fading background signal intensity (SI), especially in high b-value images [10]. The acquired DWI images were often post-processed using the standard monoexponential fit, which applies a linear shape to obtain apparent diffusion coefficient (ADC) maps. Quantitative ADC values were considered to reflect the tissue cell size and density, extracellular space viscosity and the cell framework, which limits the cellular movement of water. However, the SI decay does not fit a linear form at b values less than 200 [11, 12] or over 1,000 s/mm^2 [13, 14]. Accordingly, the non-Gaussian water diffusivity analysis using diffusion kurtosis imaging (DKI) more appropriately reflected the SI decay. Two parameters, D and K, which are produced from the DKI model, represented the diffusion coefficient and the diffusional kurtosis, respectively, and they provided more information on the tissue structure than DWI. D was assumed to be more accurate than ADC for tissue diffusion due to its correction for non-Gaussian diffusion behaviour. The parameter K was supported by observations of the DKI model fitting the SI decay at ultrahigh b values. Increased K values were suggested to be sensitive to more irregular and heterogeneous cellular environments, including the intracellular architecture, but less sensitive to cell density

[14]. Research still needs to be conducted to completely understand the biophysics of K values in tissue. The DKI model was first represented in brain imaging but has been gradually applied to extracranial organs [15–19]. Recently, DKI studies performed for head and neck cancers [16] suggested that the DKI-derived parameters were superior to conventional monoexponential DWI for differentiating between benign and malignant neoplasms and predicting treatment response. However, DKI studies have not been performed for thyroid lesions.

The purpose of this study was to investigate not only the utility of DKI in thyroid lesions compared to DWI but also the association of DKI parameters with histopathological factors and laboratory biomarkers.

Materials and methods

Patient selection

This prospective study was approved by the local institutional review board, and written informed consent was obtained from patients. Between October 2015 and June 2016, 60 consecutive patients with thyroid nodules detected by US and diagnosed as Thyroid Imaging Report and Data System (TI-RADS) category 4 in our institution who were reluctant to undergo biopsy were selected to undergo the MRI

Table 2 Characteristics of the patients and lesions

	N	Gender (F/M)	Age (years)	Size (mm, mean ± SD)
Malignant (PTC)	24	20/4	42.79 ± 11.68	13.75 ± 6.07
LN metastasis	9	8/1	35.33 ± 4.98	16.44 ± 8.56
None metastasis	15	12/3	46.75 ± 12.11	13.06 ± 4.93
Benign	34	27/7	51.76 ± 13.55	19.85 ± 6.44
Adenoma	21	16/5	48.24 ± 15.12	19.48 ± 6.04
Nodular goitre	7	6/1	58.00 ± 10.10	22.00 ± 6.73
Hashimoto thyroiditis	6	5/1	56.83 ± 5.38	18.67 ± 8.04

PTC papillary thyroid carcinoma

Table 3 Apparent diffusion coefficient (ADC) and diffusion kurtosis imaging (DKI) parameters and pathology results for each group

	ADC (10^{-3} mm²/s)	DKI D (10^{-3} mm²/s)	DKI K	Cell density	Ki-67 No. (+)	VEGF No. (+)
Malignant (PTC)	0.99 ± 0.27*	1.33 ± 0.44*	1.44 ± 0.51*	1444.38 ± 292.46*	6.49 ± 9.46*	1440.11 ± 302.96*
	P = 0.001	P = 0.000	P = 0.014	P = 0.000	P = 0.014	P = 0.000
Lymph node metastasis	0.97 ± 031	1.26 ± 0.48	1.33 ± 0.43	1431.62 ± 182.82	10.16 ± 11.63	1431.62 ± 182.82
None metastasis	1.02 ± 0.26	1.36 ± 0.42	1.52 ± 0.54	1404.73 ± 385.94	4.03 ± 7.30	1357.75 ± 495.25
Benign	1.29 ± 0.33	2.13 ± 0.77	1.09 ± 0.53	663.64 ± 251.34	1.17 ± 3.42	263.87 ± 327.37
Adenoma	1.39 ± 0.27¶	2.39 ± 0.72§	0.92 ± 0.40	670.05 ± 174.35	1.74 ± 4.28	393.86 ± 350.88Φ
Nodular goitre	1.24 ± 0.38	1.67 ± 0.50	1.31 ± 0.67	414.17 ± 102.12ø	0.14 ± 0.15	11.49 ± 5.51
Hashimoto thyroiditis	0.99 ± 0.29	1.77 ± 0.88	1.44 ± 0.58	932.27 ± 330.04	0.37 ± 0.20	103.37 ± 154.22

All data are given mean ± standard deviation

* Compared to benign groups

¶ Compared to Hashimoto thyroiditis P = 0.015

§ Compared to Nodular goitre P = 0.044

Ø Compared to Hashimoto thyroiditis P = 0.002

Φ Compared to Nodular goitre P = 0.022

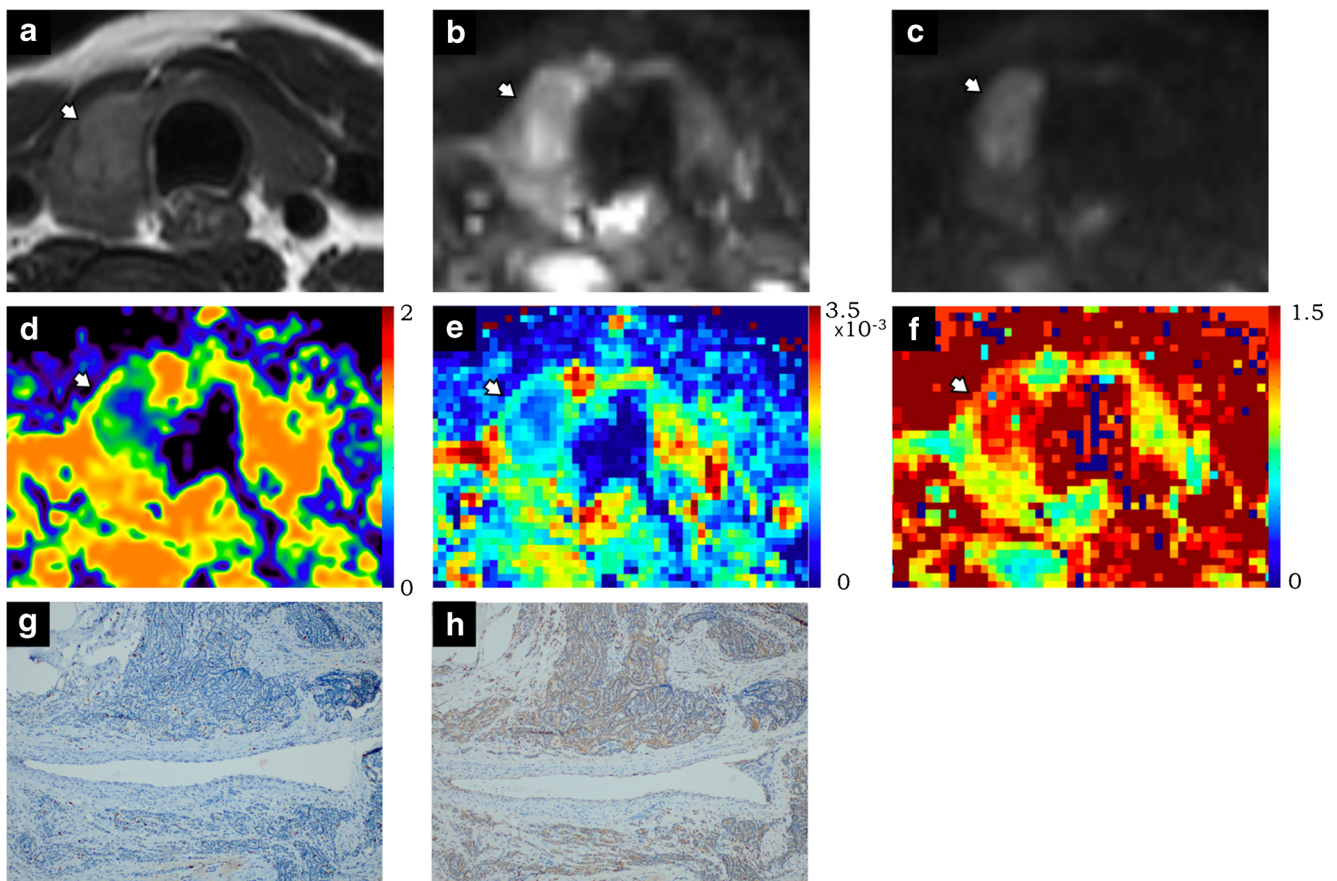*PTC* papillary thyroid carcinoma

Fig. 1 Images from a 35-year-old male patient with papillary thyroid carcinoma (PTC) in the right lobe. **a** T2-weighted image. **b** Diffusion-weighted imaging (DWI) image (b = 0). **c** DWI image (b = 750). **d** Apparent diffusion coefficient (ADC) map, ADC value = 0.786°10⁻³ mm²/s. **e** D map, D value = 1.329°10⁻³ mm²/s. **f** K map, K value = 1.045. **g** Histopathological Ki-67 expression image (total magnification, 100), Cell density = 1,511.2, Ki-67 (+) cell No. = 24.4. **f** Histopathological vascular endothelial growth factor (VEGF) expression image (total magnification, 100), VEGF (+) cell No. = 1,511.2

examination. None of the patients had other head and neck disease. Thyroidectomy was performed within 5 days after MRI. Two patients were excluded due to motion artefacts.

MR imaging

Thyroid MRI was performed with a 3.0 T unit (Ingenia, Philips Healthcare, Best, The Netherlands) and a pair of ds Flex M circular coils. Velcro straps were used to affix the coils to the anterior portion of the neck while the patient was in a comfortable supine position. The images obtained included axial T1, T2-weighted imaging, conventional DWI with b values of 0 and 750 s/mm^2 and DKI with b values of 0, 500, 1,000, 1,500 and 2,000 s/mm^2. The chosen b values were established by pretesting for sufficient signal-to-noise ratio (SNR) to observe the thyroid even in the image acquired at the highest b value. A calibration scan was performed before scanning to reduce Nyquist (N/2) ghosting artefacts. The parameters of two diffusion sequences are summarized in Table 1.

Image analysis

DWI sequence post-processing was completed at the workstation (IntelliSpace Portal, Philips Healthcare). ADC maps were generated from conventional DWI sequences with two b values that fit the monoexponential model. DKI images were transferred to a PC and post-processed using in-house software written in Matlab (version R2014b; MathWorks, Natick, MA, USA). The multi-b DWI images fitted the DKI signal decay equation: $S(b)=S_0 \cdot exp(-b \cdot D+1/6 \cdot b^2 D^2 K)$. A nonlocal-means filter for image denoising was employed before curve fitting to improve SNR. In this equation, S_o is the SI when b = 0 s/mm^2; S(b) is the SI measured at the corresponding b value; D is the diffusion coefficient; and K is kurtosis, which suggest that the status of water molecular motion deviates from a Gaussian distribution. A minimum K value showed that the curve fit closely to a Gaussian distribution. However, increased K indicated increased contributions of the lesion area attributable to kurtosis behaviour.

All images were separately analysed by two radiologists who specialized in head and neck imaging (one with 2 years'
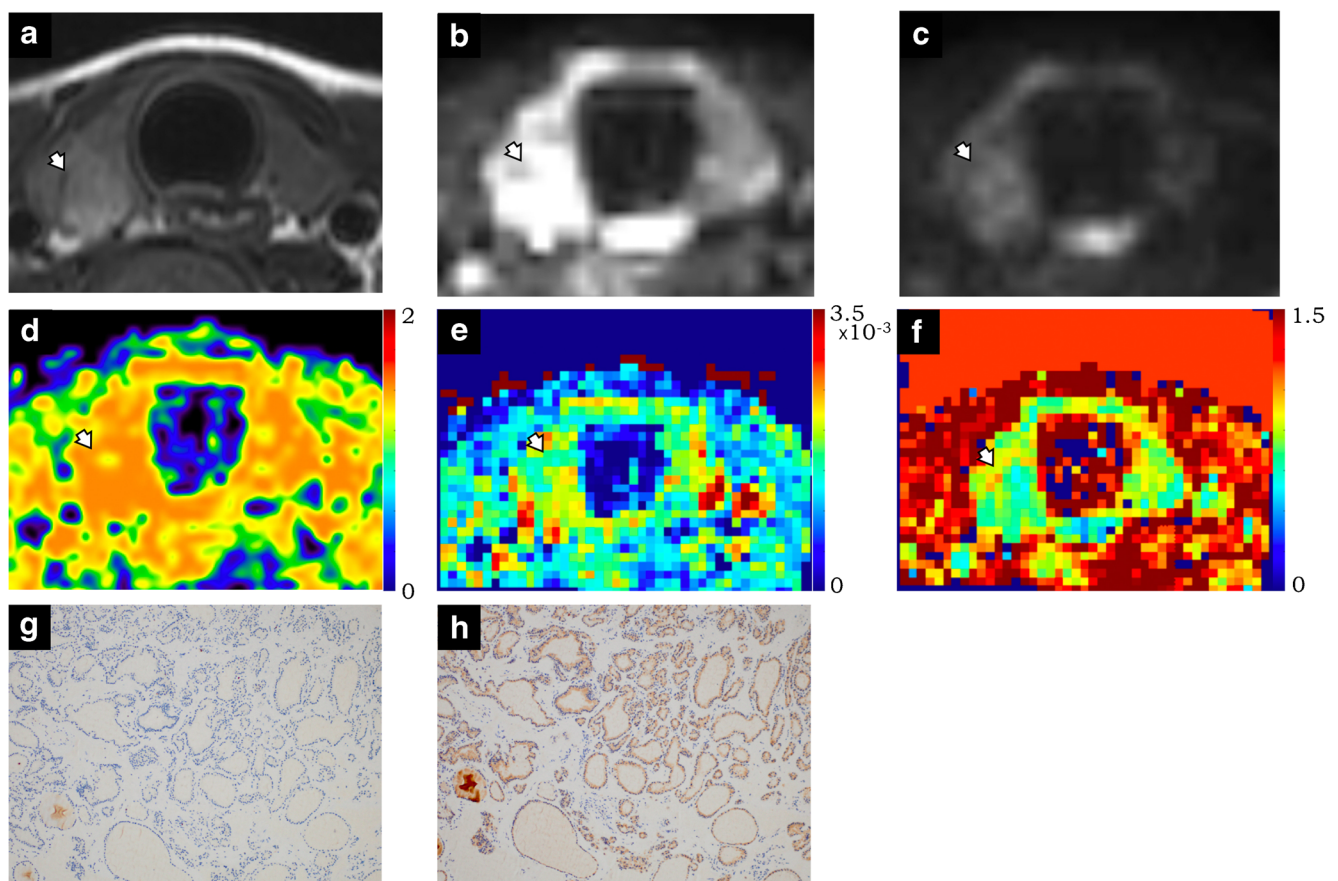

Fig. 2 Images from a 41-year-old female patient with adenoma in the right lobe. **a** T2-weighted image. **b** Diffusion-weighted imaging (DWI) image (b = 0). **c** DWI image (b = 750). **d** Apparent diffusion coefficient (ADC) map, ADC value = 1.515°10^{-3} mm^2/s. **e** D map, D value = 2.010°10^{-3} mm^2/s. **f** K map, K value = 0.779. **g** Histopathological Ki-67 expression image (total magnification, 100), cell density = 817.6, Ki-67 (+) cell No. = 0.4. **f** Histopathological vascular endothelial growth factor (VEGF) expression image (total magnification, 100), VEGF (+) cell No. = 817.6

and another with 7 years' experience) blinded to the clinical and ultrasound diagnosis. The region of interest (ROI) was drawn on ADC maps and copied to D maps and K maps for each lesion, avoiding obvious cysts, calcifications and the margins of the lesion.

Histopathological analysis

The pathological diagnosis was based on a haematoxylin and eosin (HE)-stained section. VEGF (1/200 dilution, Thermo Fisher, Waltham, MA, USA) and Ki-67 (1/200 dilution, Dako, Demark) staining for immunohistochemical analysis were performed on 4-μm sections of paraffin-embedded tissues to observe protein expression levels. Positive and negative controls were used for the tested antibodies. Images of five randomly high-power fields (HPFs, magnification × 400) in the lesion area were selected to count total cells and positively stained cells. Cell numbers were calculated as the average of five HPFs for statistical analysis. All the histopathological section analyses were performed using a microscope (Carl

Zeiss, Jena, Germany) by one pathologist with 10 years of experience in pathological diagnosis.

Statistical analysis

An independent samples t-test was used to compare the ADC, D and K values of benign lesions with malignant lesions. One-way analysis of variance (ANOVA) with Tukey's honest significance test as a post hoc analysis was used to analyse the variance of ADC, D and K among subgroups. The receiver operating characteristic (ROC) curve analysis was used to determine the threshold values of ADC, D and K to differentiate between benign and malignant thyroid lesions. Pearson's correlation analysis was used to evaluate the association of diffusion parameters with histopathological factors. A P-value less than 0.05 was considered statistically significant. The previously mentioned statistical analyses were performed with IBM SPSS Statistics 22.0 software. The inter-observer agreements between two observers were described on Bland-Altman plots using Medcalc software (Medcalc Version 17.2, Medcalc Software, Ostend, Belgium).
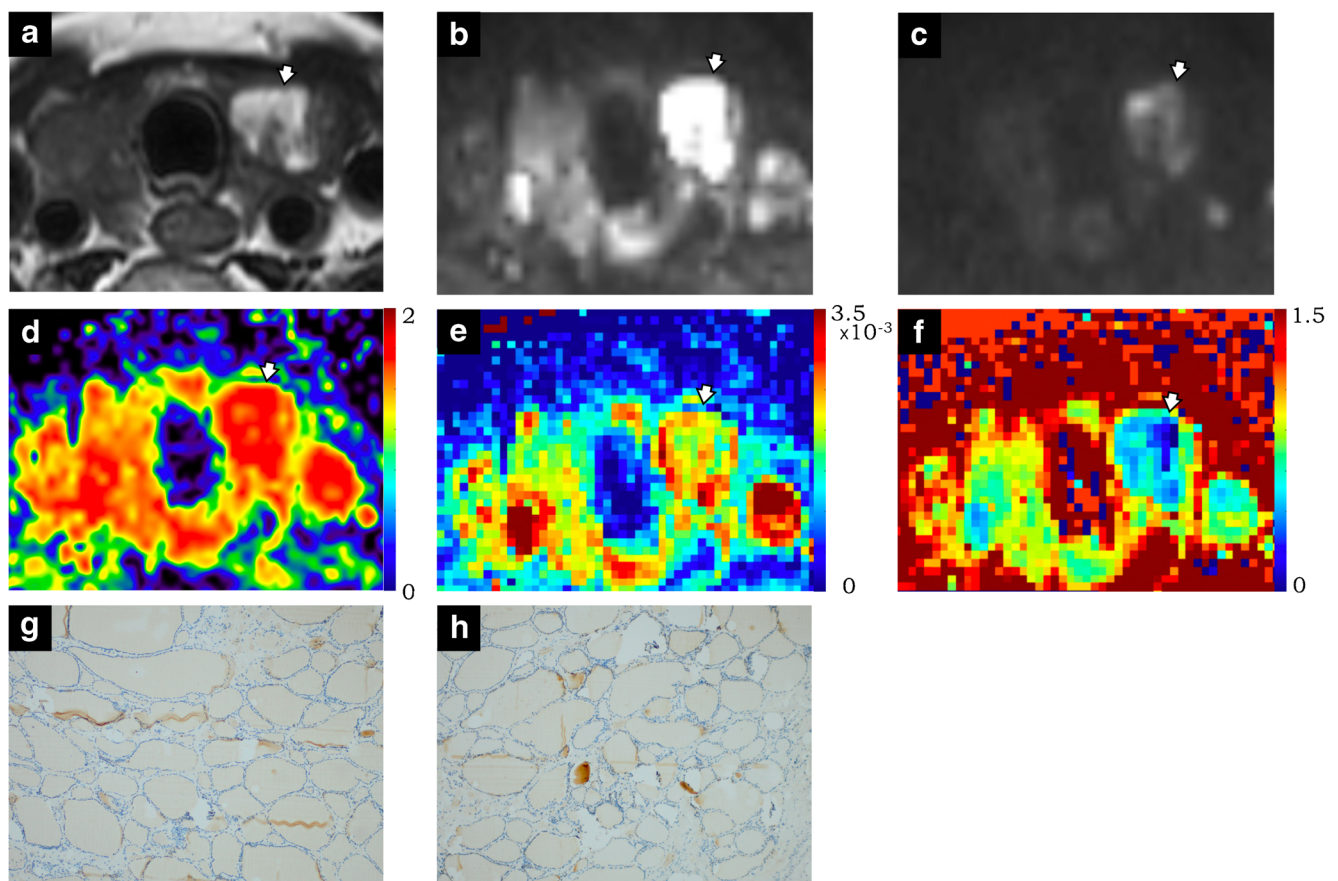

Fig. 3 Images from a 65-year-old female patient with nodular goitres in both lobe. **a** T2-weighted image. **b** Diffusion-weighted imaging (DWI) image (b = 0). **c** DWI image (b = 750). **d** Apparent diffusion coefficient (ADC) map, ADC value = $1.885°10^{-3}$ mm^2/s. **e** D map, D value = $2.296°10^{-3}$ mm^2/s. **f** K map, K value = 0.490. **g** Histopathological Ki-67 expression image (total magnification, 100), Cell density = 313.8, Ki-67 (+) cell No. = 0.2. **f** Histopathological vascular endothelial growth factor (VEGF) expression image (total magnification, 100), VEGF (+) cell No. = 17

Results

Of the 58 patients (mean age 48.05 ± 13.46 years), 58 lesions (mean size 17.33 ± 6.93 mm) were found, including 24 PTC, 21 adenomas, seven nodular goitres and six cases of Hashimoto's thyroiditis. In the 24 PTC cases, nine patients were found to have lymph node metastasis. The characteristics of the remaining 58 patients and the lesions are summarized in Table 2. The three diffusion parameters and the histopathological factors of each group are shown in Table 3. The average ADC values and D values of malignant lesions were significantly lower than those of benign ones (P < 0.001, P < 0.001). Malignant lesions have significantly higher average K values than benign lesions (P = 0.014). Cell density and the number of positively stained VEGF cell numbers were significantly higher in the malignant group (P < 0.001, P < 0.001). The positively stained Ki-67 cell numbers were significantly higher in the malignant group (P = 0.004). However, even in the malignant group, Ki-67 expression levels were too low to meet the clinical threshold value of 5%. In the subgroup analysis of the malignant lymph node metastasis and no metastasis groups, no statistically significant differences were found for any parameters. The statistical analysis of the benign groups was relatively complicated. The ADC value of the adenoma group was significantly higher than the Hashimoto's thyroiditis group (1.39 ± 0.27 vs. 0.99 ± 0.29, P = 0.015); the D value of the adenoma group was significantly higher than the nodular goitre group (2.39 ± 0.72 vs. 1.67 ± 0.50, P = 0.044); the cell density of the nodular goitre group was significantly lower than the Hashimoto's thyroiditis group (414.17 ± 102.12 vs. 932.27 ± 330.04, P = 0.002); and the positively stained VEGF cell number of the adenoma group was significantly higher than the nodular goitre group (393.86 ± 350.88 vs. 11.49 ± 5.51, P = 0.022). Four samples of PTC, adenoma, nodular goitre and Hashimoto's thyroiditis cases are shown in Figs. 1, 2, 3 and 4.

The results of ROC analyses for differentiating malignant thyroid lesions from benign ones using three diffusion parameters are summarized in Fig. 5 and Table 4. The area under the curve (AUC) for D (0.797) was significantly greater than the AUC for K (0.797 vs. 0.701, P = 0.0218), and the AUC of
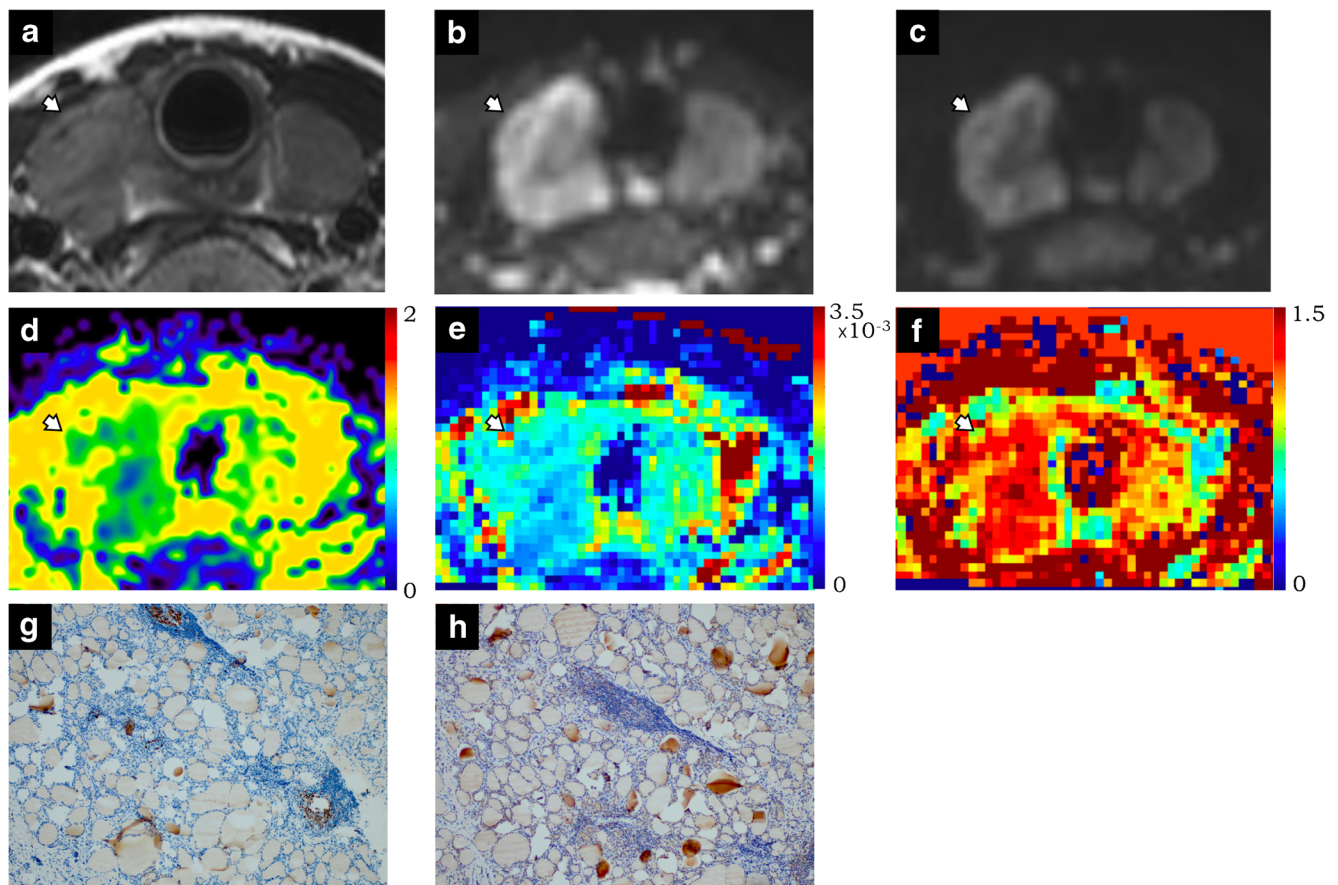

Fig. 4 Images from a 48-year-old female patient with Hashimoto thyroiditis in both lobe. **a** T2-weighted image. **b** Diffusion-weighted imaging (DWI) image (b = 0). **c** DWI image (b = 750). **d** Apparent diffusion coefficient (ADC) map, ADC value = 0.735°10^{-3} mm^2/s. **e** D map, D value = 1.145°10^{-3} mm^2/s. **f** K map, K value = 1.065. **g** Histopathological Ki-67 expression image (total magnification, 100), cell density = 1,132, Ki-67 (+) cell No. = 0.6. **f** Histopathological vascular endothelial growth factor (VEGF) expression image (total magnification, 100), VEGF (+) cell No. = 17.6
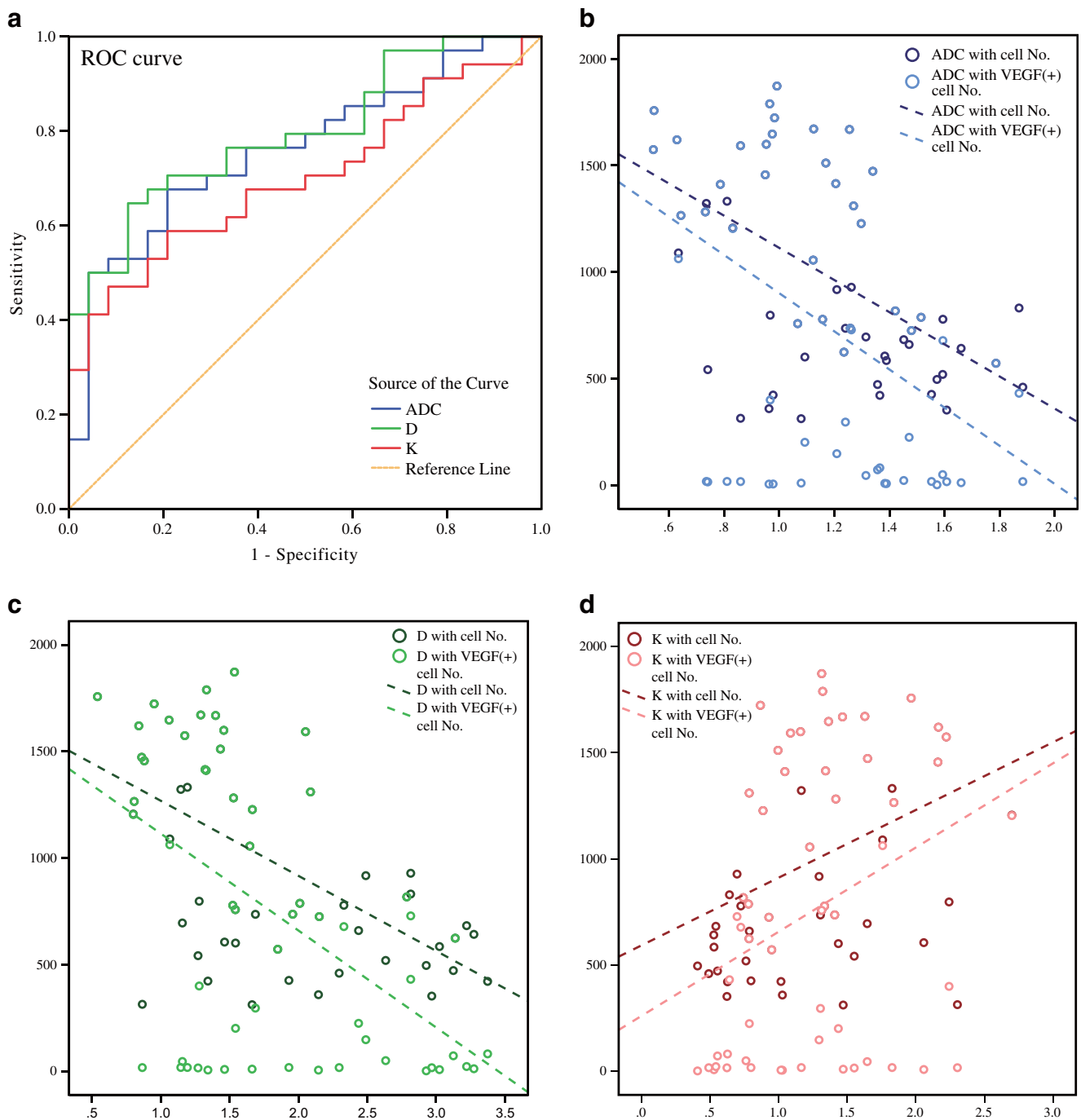
Fig. 5 **a** ROC curve to discriminate papillary thyroid carcinoma (PTC) and benign thyroid nodules using apparent diffusion coefficient (ADC), D and K. **b**, **c**, **d** Scatter plots of ADC (10^{-3} mm^2/s), D (10^{-3} mm^2/s) and K versus cell density and vascular endothelial growth factor (VEGF) expression positive cell number

ADC was between those of D and K. The greatest sensitivity was obtained for K (0.917), while the greatest specificity was shown for ADC (0.676).

The correlation of diffusion parameters and histopathological factors are summarized in Table 5 and Fig. 5. Pearson's correlation coefficient between D and cell density was relatively greater (−0.570, P < 0.001); the correlation between D and the number of positively stained VEGF cells is −0.522 (P < 0.001); the correlation coefficient between ADC and cell density was −0.536 (P < 0.001). Bland-Altman plots for ADC, D and K value of all patients are shown in Fig. 6 and indicate good inter-observer agreement.

Table 4 Area under the receiver operating characteristic curve (AUC), threshold, sensitivity and specificity of ADC, DKI D, and DKI K

Parameter	AUC	Threshold	Sensitivity	Specificity
ADC	0.762	≤1.207	0.792	0.676
DKI D	0.797	≤1.676	0.875	0.647
DKI K	0.701	≥0.832	0.917	0.471

ADC apparent diffusion coefficient, *DKI* diffusion kurtosis imaging

Discussion

DWI has been used for decades to differentiate thyroid malignancies from benign lesions [5, 9, 20–32]. Most previous studies indicated that the ADC value decreased in malignant lesions and showed considerable diagnostic accuracy. In recent years, researchers have also tried to improve the image quality for DWI images [4]. In our study, we selected flex coils with fixed straps and performed a B1 calibration scan before scanning. Additionally, we added averages of high b values to reduce artefacts and obtain sufficient SNR. Before DKI curve fitting, we used a nonlocal-means filter to further improve SNR. Thus, DKI analysis of the thyroid was manageable. We also analysed the inter-observer variability by using Bland-Altman plots for ADC- and DKI-deprived parameters between two observers. The good inter-observer agreement enhanced the credibility of the study.

Our study indicated that quantitative DKI was superior to conventional DWI because the D corrected by the DKI model showed greater AUC than ADC, and K showed higher sensitivity than the ADC value. The combination of multiple parameters would provide higher diagnostic accuracy. Our study also compared the subgroups of malignancies and benign lesions and reached interesting results: In the malignant group, the diffusion parameter and histopathological factors showed no statistically significant differences between the two subgroups with or without lymph node metastasis; in the benign group, the ADC value

Table 5 Correlation coefficient of diffusion parameters with histopathological results

	Cell density	Ki-67 No. (+)	VEGF No. (+)
ADC	-0.536*	-0.081	-0.451*
	P = 0.000	P = 0.547	P = 0.000
DKI D	-0.570*	-0.158	-0.522*
	P = 0.000	P = 0.236	P = 0.000
DKI K	0.370*	-0.154	0.326*
	P = 0.004	P = 0.248	P = 0.012

VEGF vascular endothelial growth factor, *ADC* apparent diffusion coefficient, *DKI* diffusion kurtosis imaging

of Hashimoto's thyroiditis was significantly lower than adenoma, but this difference was not shown in the D values. For the three diffusion parameters, the highest sensitivity was acquired at K. The combination of D and K in DKI would obtain better diagnostic accuracy than conventional DWI.

Current research appears to validate the view that DWI and ADC values reflect the histopathological changes of thyroid tissue [5, 8, 9]. Shi et al. [9] proved the correlation between cell density and relatively severe desmoplastic response with ADC values in thyroid cancer. Lu et al. [5] used DWI to predict the aggressiveness of histological features in PTC and found that patients with extrathyroidal extension (ETE) showed significantly lower ADC values than PTCs without ETE. Schob et al. [8] analysed the subtypes of thyroid carcinoma with readout-segmented multishot EPI sequence DWI and compared them with cell density, Ki-67 index and p53 index. In our study, we also performed histopathological studies to explore the association of the lesion structure with diffusion parameters. Increased cell density in lesions restricted water diffusion in the extracellular space. Ki-67 is a cell proliferation protein that is considered a neoplastic marker to help diagnose differentiated thyroid carcinoma (DTC) [33] as well as predict disease-free survival (DFS) and cause-specific survival (CSS) in patients [34]. VEGF is a cytokine that induces angiogenesis and is related to lymphangiogenesis. The high expression of VEGF indicated the growth of tumour-associated vessels and lymph node metastasis [35, 36].

In our study, we analysed the cell density and the expression of Ki-67 and VEGF compared with the DWI and DKI parameters. The cell density, Ki-67 and VEGF expression of the malignant group were significantly higher than the benign group. However, in all the PTC cases, the Ki-67 labelling index was too low (less than 10%) to be considered to represent strong expression. This expression level was lower than in some previous studies [8, 33] but was similar to the study by Radu et al. [37]. No significant differences were found in all the parameters when comparing the PTC and the lymph node metastasis group with the no metastasis group. In the benign group, Hashimoto's thyroiditis lesions showed significantly lower ADC values compared to the adenoma group for the relative cell density and abundant irregular lymphocytes; the Ki-67 expression stayed low in all groups, and the expression of VEGF in adenoma was significantly higher compared with nodular goitre.

The correlations evaluated between diffusion parameters and histopathological parameters were as follows: there were moderate correlations between cell density and diffusion parameters, especially D values; the correlation of D and VEGF was also the highest among the three diffusion parameters with VEGF analysis. K showed a low correlation with cell density and VEGF expression. These
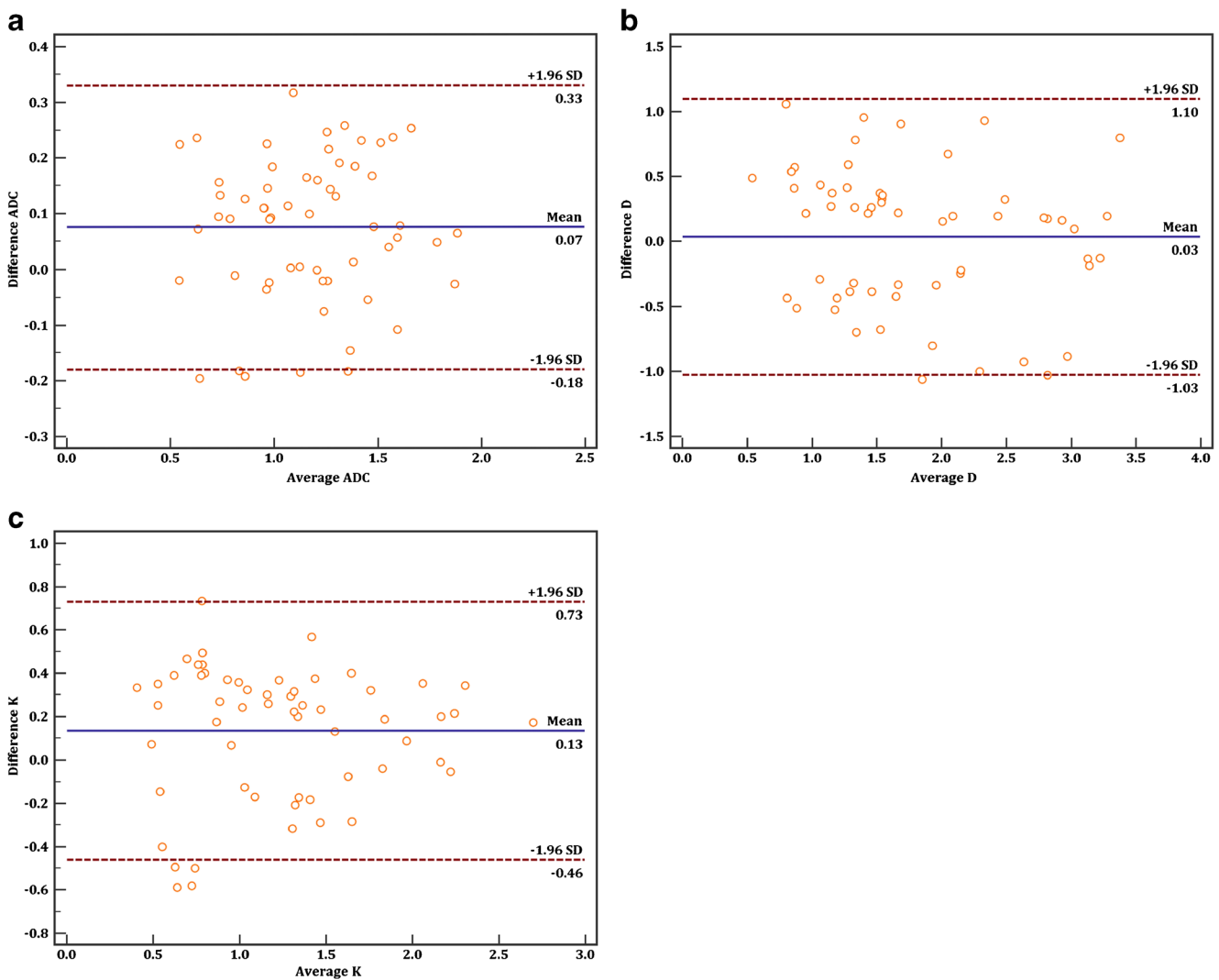
Fig. 6 Bland-Altman plots show the inter-observer analysis between two observers, such as (**a**) apparent diffusion coefficient (ADC) value, (**b**) D value and (**c**) K value. The solid lines represent the mean difference and the dotted lines represent the 95% limits of agreement

phenomena (ADC and D) were correlated with extracellular changes; K was more sensitive to intracellular architecture but not overall cell density [14]. This presumed result still requires more studies to understand the mechanisms.

Our study has a few limitations. First, this is a preliminary study, and only a small number of PTCs, especially cases with metastasis, Hashimoto's thyroiditis and other kinds of malignant thyroid carcinoma, were included. Second, the single-shot echo planar imaging-based DWI adopted in our study is the most commonly used technique in the clinical setting. Although we have attempted methods to improve SNR, alternative techniques, such as multiple-shot spin echo DWI and readout-segmented multi-shot echo planar imaging, can reduce the artefacts. Third, since b values less than 200 s/mm^2 were not adopted in the diffusion sequence, the biexponential model cannot be compared to the DKI model and histopathological results. Finally, the immunohistochemical analysis of thyroid lesion may provide an explanation to a certain extent,

but further research still needs to be conducted to understand the meaning of the DKI model.

In conclusion, the DKI-derived parameters D and K demonstrated advantages compared to conventional DWI for thyroid lesion diagnosis. While the histopathological study indicated that the D value corrected by DKI model correlated better with extracellular changes than ADC values, the changes in K values related to the intracellular structure still require further study.

Compliance with ethical standards

Guarantor The scientific guarantor of this publication is Jian-rong Xu, Department of Radiology, Ren Ji Hospital, School of Medicine, Shanghai Jiao Tong University.

References

1. Siegel RL, Miller KD, Jemal A (2016) Cancer statistics, 2016. CA Cancer J Clin 66:7–30

2. Yoon JH, Lee HS, Kim EK, Moon HJ, Kwak JY (2015) Thyroid nodules: nondiagnostic cytologic results according to thyroid imaging reporting and data system before and after application of the bethesda system. Radiology 142308

3. Ilica AT, Artaş H, Ayan A et al (2013) Initial experience of 3 tesla apparent diffusion coefficient values in differentiating benign and malignant thyroid nodules. J Magn Reson Imaging 37:1077–1082

4. Lu Y, Hatzoglou V, Banerjee S et al (2015) Repeatability investigation of reduced field-of-view diffusion-weighted magnetic resonance imaging on thyroid glands. J Comput Assist Tomogr 39:334–339

5. Lu Y, Moreira AL, Hatzoglou V et al (2015) Using diffusion-weighted MRI to predict aggressive histological features in papillary thyroid carcinoma: a novel tool for pre-operative risk stratification in thyroid cancer. Thyroid 25:672–680

6. Merisaari H, Toivonen J, Pesola M et al. (2015) Diffusion-weighted imaging of prostate cancer: effect of b-value distribution on repeatability and cancer characterization. Magn Reson Imaging

7. Politi LS, Godi C, Cammarata G et al (2014) Magnetic resonance imaging with diffusion-weighted imaging in the evaluation of thyroid-associated orbitopathy: getting below the tip of the iceberg. Eur Radiol 24:1118–1126

8. Schob S, Voigt P, Bure L et al (2016) Diffusion-weighted imaging using a readout-segmented, multishot EPI sequence at 3 T distinguishes between morphologically differentiated and undifferentiated subtypes of thyroid carcinoma—a preliminary study. Transl Oncol 9:403–410

9. Shi HF, Feng Q, Qiang JW, Li RK, Wang L, Yu JP (2013) Utility of diffusion-weighted imaging in differentiating malignant from benign thyroid nodules with magnetic resonance imaging and pathologic correlation. J Comput Assist Tomogr 37:505–510

10. Woodhams R, Ramadan S, Stanwell P et al (2011) Diffusion-weighted imaging of the breast: principles and clinical applications. Radiographics 31:1059–1084

11. Cho GY, Moy L, Zhang JL et al (2016) Evaluation of breast cancer using intravoxel incoherent motion (IVIM) histogram analysis: comparison with malignant status, histological subtype, and molecular prognostic factors. Eur Radiol 26:2547–2558

12. Cho GY, Moy L, Zhang JL et al (2015) Comparison of fitting methods and b-value sampling strategies for intravoxel incoherent motion in breast cancer. Magn Reson Med 74:1077–1085

13. Jensen JH, Helpern JA, Ramani A, Lu H, Kaczynski K (2005) Diffusional kurtosis imaging: the quantification of non-gaussian water diffusion by means of magnetic resonance imaging. Magn Reson Med 53:1432–1440

14. Rosenkrantz AB, Padhani AR, Chenevert TL (2015) Body diffusion kurtosis imaging: basic principles, applications, and considerations for clinical practice. J Magn Reson Imaging 42:1190–1202

15. Iima M, Yano K, Kataoka M et al (2015) Quantitative non-Gaussian diffusion and intravoxel incoherent motion magnetic resonance imaging: differentiation of malignant and benign breast lesions. Investig Radiol 50:205–211

16. Jiang JX, Tang ZH, Zhong YF, Qiang JW (2016) Diffusion kurtosis imaging for differentiating between the benign and malignant sinonasal lesions. J Magn Reson Imaging

17. Sun K, Chen X, Chai W et al. (2015) Breast cancer: diffusion kurtosis MR imaging-diagnostic accuracy and correlation with clinical-pathologic factors. Radiology 141625

18. Suo S, Chen X, Wu L et al (2014) Non-Gaussian water diffusion kurtosis imaging of prostate cancer. Magn Reson Imaging 32:421–427

19. Wu D, Li G, Zhang J, Chang S, Hu J, Dai Y (2014) Characterization of breast tumors using diffusion kurtosis imaging (DKI). PLoS One 9:e113240

20. Abdel Razek AA, Sadek AG, Gaballa G (2010) Diffusion-weighed MR of the thyroid gland in Graves' disease: assessment of disease activity and prediction of outcome. Acad Radiol 17:779–783

21. Bozgeyik Z, Coskun S, Dagli AF, Ozkan Y, Sahpaz F, Ogur E (2009) Diffusion-weighted MR imaging of thyroid nodules. Neuroradiology 51:193–198

22. Chen L, Xu J, Bao J et al (2016) Diffusion-weighted MRI in differentiating malignant from benign thyroid nodules: a meta-analysis. BMJ Open 6:e8413

23. Dilli A, Ayaz UY, Cakir E, Cakal E, Gultekin SS, Hekimoglu B (2012) The efficacy of apparent diffusion coefficient value calculation in differentiation between malignant and benign thyroid nodules. Clin Imaging 36:316–322

24. Erdem G, Erdem T, Muammer H et al (2010) Diffusion-weighted images differentiate benign from malignant thyroid nodules. J Magn Reson Imaging 31:94–100

25. Mutlu H, Sivrioglu AK, Sonmez G et al (2012) Role of apparent diffusion coefficient values and diffusion-weighted magnetic resonance imaging in differentiation between benign and malignant thyroid nodules. Clin Imaging 36:1–7

26. Nakahira M, Saito N, Murata S et al (2012) Quantitative diffusion-weighted magnetic resonance imaging as a powerful adjunct to fine needle aspiration cytology for assessment of thyroid nodules. Am J Otolaryngol 33:408–416

27. Razek AA, Sadek AG, Kombar OR, Elmahdy TE, Nada N (2008) Role of apparent diffusion coefficient values in differentiation between malignant and benign solitary thyroid nodules. Am J Neuroradiol 29:563–568

28. Sasaki M, Sumi M, Kaneko K (2013) Multiparametric MR imaging for differentiating between benign and malignant thyroid nodules: Initial experience in 23 patients. J Magn Reson Imaging 38:64–71

29. Schueller-Weidekamm C, Kaserer K, Schueller G et al (2008) Can quantitative diffusion-weighted MR imaging differentiate benign and malignant cold thyroid nodules? Initial results in 25 patients. Am J Neuroradiol 30:417–422

30. Taviani V, Nagala S, Priest AN, McLean MA, Jani P, Graves MJ (2013) 3T diffusion-weighted MRI of the thyroid gland with reduced distortion: preliminary results. Br J Radiol 86:20130022

31. Wu LM, Chen XX, Li YL et al (2014) On the utility of quantitative diffusion-weighted MR imaging as a tool in differentiation between malignant and benign thyroid nodules. Acad Radiol 21:355–363

32. Wu Y, Yue X, Shen W et al (2013) Diagnostic value of diffusion-weighted MR imaging in thyroid disease: application in differentiating benign from malignant disease. BMC Med Imaging 13:23

33. Maia FF, Vassallo J, Pinto GA, Pavin EJ, Matos PS, Zantut-Wittmann DE (2016) Expression of Mcl-1 and Ki-67 in papillary thyroid carcinomas. Exp Clin Endocrinol Diabetes 124:209–214

34. Ito Y, Miyauchi A, Kakudo K, Hirokawa M, Kobayashi K, Miya A (2010) Prognostic significance of Ki-67 labeling index in papillary thyroid carcinoma. World J Surg 34:3015–3021

35. Gulubova M, Ivanova K, Ananiev J et al (2014) VEGF expression, microvessel density and dendritic cell decrease in thyroid cancer. Biotechnol Biotechnol Equip 28:508–517

36. Yasuoka H, Nakamura Y, Zuo H et al (2005) VEGF-D expression and lymph vessels play an important role for lymph node metastasis in papillary thyroid carcinoma. Mod Pathol 18:1127–1133

37. Radu TG, Mogoantă L, Busuioc CJ, Stănescu C, Grosu F (2015) Histological and immunohistochemical aspects of papillary thyroid cancer. Romanian J Morphol Embryol 56:789–795